Available online at www.sciencedirect.com
ScienceDirect
Journal of Solid State Chemistry 179 (2006) 3958–3964
JOURNAL OF SOLID STATE CHEMISTRY
www.elsevier.com/locate/jssc

The non-centrosymmetric borate oxides, MBi$_2$B$_2$O$_7$ (M = Ca, Sr)

J. Barbier[a,*], L.M.D. Cranswick[b]

[a]Department of Chemistry, McMaster University, Hamilton, Ont., Canada L8S4M1
[b]Canadian Neutron Beam Centre, National Research Council Canada, Chalk River, Ont., Canada K0J 1J0

Received 13 July 2006; received in revised form 28 August 2006; accepted 31 August 2006
Available online 12 September 2006

Abstract

Two novel noncentrosymmetric borates oxides, MBi$_2$B$_2$O$_7$ or MBi$_2$O(BO$_3$)$_2$ (M = Ca, Sr), have been synthesized by solid-state reactions in air at temperatures in the 600–700 °C range. Their crystal structures have been determined ab initio and refined using powder neutron diffraction data. CaBi$_2$B$_2$O$_7$ crystallizes in the orthorhombic $Pna2_1$ space group with $a = 8.9371(5)$ Å, $b = 5.4771(3)$ Å, $c = 12.5912(7)$ Å, $Z = 4$, $R_{wp} = 0.118$, $\chi^2 = 2.30$. SrBi$_2$B$_2$O$_7$ crystallizes in the hexagonal $P6_3$ space group with $a = 9.1404(4)$ Å, $c = 13.0808(6)$ Å, $Z = 6$, $R_{wp} = 0.115$, $\chi^2 = 4.15$. Large displacement parameters suggest the presence of disorder in SrBi$_2$B$_2$O$_7$ as also revealed by diffuse $2 \times a$ superstructure reflections in electron diffraction patterns. Both structures are built of identical (001) neutral layers of corner-sharing BO$_3$ triangles and MO$_6$ trigonal prisms forming six-membered rings in which Bi$_2$O groups are located. Adjacent layers are stacked in a staggered configuration and connected through weak Bi–O bonds. A moderate efficiency for second harmonic generation (SHG) has been measured for a powder sample of CaBi$_2$B$_2$O$_7$ ($d_{eff} = 2d_{eff}$(KDP)).

Keywords: CaBi$_2$B$_2$O$_7$; SrBi$_2$B$_2$O$_7$; Borates; Borate oxides; Crystal structure; Powder neutron diffraction; ab initio structure determination; Rietveld refinement; FOX software

1. Introduction

The excellent nonlinear optical (NLO) properties of the non-centrosymmetric α-BiB$_3$O$_6$ compound [1–4], have generated continuing interest in crystalline and glassy bismuth borates as potential NLO materials. The binary Bi borates that have been synthesized and characterized to date include BiBO$_3$ [5], Bi$_4$B$_2$O$_9$ [6,7], Bi$_2$B$_8$O$_{15}$ [8], Bi$_3$B$_5$O$_{12}$ [9] and, just reported in the past year, centrosymmetric β- and γ-BiB$_3$O$_6$ [10], as well as BiB$_2$O$_4$F, BiB$_4$O$_6$(OH)$_3$ and Bi$_3$B$_6$O$_{13}$(OH) [11]. Depending on the details of the crystal structures, the asymmetric BiO$_n$ coordination polyhedra and/or the borate groups are thought to be the main contributors to the NLO properties of the non-centrosymmetric Bi borates (e.g. [2,11]).

Besides the binary compounds, only a limited number of ternary Bi borates have been structurally characterized, including Cu$_5$Bi$_2$B$_4$O$_{14}$ [12], ZnBi$_4$B$_2$O$_{10}$ tentatively identified from powder X-ray diffraction data [13] and PbBiBO$_4$ [14]. Our own investigation of a number of MO–Bi$_2$O$_3$–B$_2$O$_3$ systems have also recently led to the characterization of several non-centrosymmetric compounds, including BaBiBO$_4$ (a new borate oxide structure-type with $Pna2_1$ symmetry) [15] and Bi$_2$ZnB$_2$O$_7$ ($Pba2$) and CaBiGaB$_2$O$_7$ (P-42$_1m$), both borate derivatives of the melilite structure-type [16]. This paper presents the results of further investigations of the CaO/SrO–Bi$_2$O$_3$–B$_2$O$_3$ systems in which two more non-centrosymmetric borate oxides, CaBi$_2$B$_2$O$_7$ and SrBi$_2$B$_2$O$_7$, have been characterized via the ab initio determination of their crystal structures using powder neutron diffraction data.

2. Experimental

The CaBi$_2$B$_2$O$_7$ and SrBi$_2$B$_2$O$_7$ compounds were discovered during exploratory syntheses in the corresponding ternary systems. All samples were synthesized via standard solid-state reactions using mixtures of Ca/Sr carbonate or nitrate, Bi$_2$O$_3$ and B(OH)$_3$ powders (99% purity or better)

*Corresponding author. Fax: +1 905 522 2509.
E-mail address: barbier@mcmaster.ca (J. Barbier).

0022-4596/$ - see front matter © 2006 Elsevier Inc. All rights reserved.
doi:10.1016/j.jssc.2006.08.037

that were pelletized and heated progressively up to temperatures in the 650–700 °C range. Polycrystalline samples corresponding to the MO:Bi_2O_3:B_2O_3 molar ratios produced single-phase products as identified by the indexing of their powder X-ray diffraction patterns (Table 1). It was established from the X-ray data that $CaBi_2B_2O_7$ crystallizes in the orthorhombic *Pnam* or $Pna2_1$ space group while $SrBi_2B_2O_7$ crystallizes in a primitive hexagonal space group without *c*-glide symmetry. Crystal growth experiments using Bi_2O_3 as a flux yielded single crystals of both compounds with sizes suitable for X-ray diffraction. However, as subsequently understood from the nature of the crystal structures (see below), crystals were generally found to be either multiply twinned or composites and, thus, not suitable for detailed structural studies. It was therefore decided instead to carry out ab initio structure determinations using high-resolution powder neutron diffraction data to obtain accurate coordinates for the positions of both light and heavy atoms in the structures.

The neutron diffraction data for $CaBi_2B_2O_7$ and $SrBi_2B_2O_7$ were collected with the C2 high-resolution powder diffractometer at the Canadian Neutron Beam Centre in Chalk River. For this purpose, large powder samples of approximately 10 g each were synthesized as described above using ^{11}B-enriched boric acid (99.3% from Eagle-Picher) in order to minimize the absorption of neutrons by ^{10}B nuclei. The two diffraction patterns were measured at room temperature in 0.05° steps over the 5–115° 2θ range by merging data collected at the low- and high-angle settings of the C2 detector.

The program FOX [17] based on a direct space global optimization method for structure solution was used to solve the crystal structures of both compounds. A major advantage of this program is the possibility to use coordination polyhedra as building blocks with dynamic occupancies of atom sites to model the connectivity of polyhedra via the sharing of corners, edges or faces. This approach is particularly useful for the solution of inorganic borate structures in which the anions are known to only consist of triangular BO_3 and/or tetrahedral BO_4 groups possibly linked into dimers, chains, rings, layers or frameworks via corner sharing only. The program requires the a priori knowledge of unit-cell parameters and space group symmetry which were derived in this case from the indexing of the powder X-ray patterns. As mentioned above, the choice of space group for $CaBi_2B_2O_7$ was limited to centric *Pnam* or acentric $Pna2_1$, and the latter was selected on the basis of the observation of a second harmonic signal generated by a powder sample in a Kurtz–Perry-type experiment (see below). Given the simple stoichiometry, two structure models were tested corresponding to either a diborate structure with dimeric tetrahedral B_2O_7 groups, or a borate oxide structure with orthoborate BO_3 groups and O atoms, i.e. $(BO_3)_2O$. The latter model was shown to be the correct choice as part of the global optimization process leading to a unit-cell content of four $CaBi_2B_2O_7$ formula units with one Ca atom, two BO_3 groups and two

Table 1
X-ray powder patterns for $CaBi_2B_2O_7$ (primitive orthorhombic, $a = 8.921(2)$ Å, $b = 5.476(1)$ Å, $c = 12.560(3)$ Å, $Z = 4$ and $SrBi_2B_2O_7$ (primitive hexagonal, $a = 9.1240(6)$ Å, $c = 13.076(2)$ Å, $Z = 6$)

h	k	l	d_{cal} (Å)	d_{obs} (Å)	I_{obs}
$CaBi_2B_2O_7$ pattern					
0	0	2	6.2802	6.2856	11
0	1	1	5.0196	5.0231	8
1	1	0	4.6668	4.6718	38
2	0	0	4.4603	4.4665	28
1	1	1	4.3746	4.3767	45
2	0	1	4.2032	4.2088	23
2	1	0	3.4583	3.4595	16
0	1	3	3.3260	3.3279	17
1	1	3	3.1164	3.1171	98
2	0	3	3.0526	3.0538	52
0	2	0	2.7379	2.7374	22
2	1	3	2.6663	2.6645	3
3	1	0	2.6131	2.6148	100
3	1	2	2.4126	2.4128	12
2	2	0	2.3334	2.3325	8
2	2	1	2.2941	2.2945	17
4	0	0	2.2302	2.2303	14
1	2	3	2.2194	2.2201	4
4	0	1	2.1958	2.1949	7
2	2	2	2.1873	2.1868	3
0	0	6	2.0934	2.0929	16
4	1	0	2.0654	2.0648	11
4	1	1	2.0381	2.0376	36
1	2	4	2.0105	2.0098	11
3	2	1	1.9887	1.9878	3
4	0	3	1.9683	1.9683	29
2	0	6	1.8950	1.8948	4
3	2	3	1.8150	1.8149	33
2	1	6	1.7908	1.7909	4
5	1	0	1.6964	1.6971	6
1	1	7	1.6748	1.6753	26
$SrBi_2B_2O_7$ pattern					
1	1	0	4.5618	4.5622	46
1	1	1	4.3070	4.3065	5
0	0	4	3.2677	3.2676	3
1	1	3	3.1508	3.1510	100
2	0	3[a]	2.9266	2.9279	2
2	1	2[a]	2.7162	2.7116	4
3	0	0	2.6337	2.6345	57
2	2	0	2.2809	2.2803	17
2	2	1	2.2469	2.2473	5
0	0	6	2.1785	2.1791	11
2	2	3	2.0207	2.0210	44
2	1	5[a]	1.9670	1.9671	9
1	1	6	1.9658		
4	1	0	1.7242	1.7240	8
3	0	6	1.6787	1.6786	22
4	1	3	1.6032	1.6029	23
4	0	5[a]	1.5760	1.5759	4
2	2	6	1.5754		
3	3	0	1.5206	1.5205	9
2	2	7	1.4449	1.4452	1
5	1	2	1.3868	1.3854	6
1	1	9	1.3839		
5	0	5[a]	1.3524	1.3529	4
4	1	6	1.3520		
6	0	0	1.3169	1.3170	7

Guinier–Hägg camera, Cu$K\alpha_1$ radiation, Si internal standard, I_{obs} measured with a KEJ line scanner.

[a]Weak reflections associated with the $(\sqrt{3} \times a, c)$ superstructure in $SrBi_2B_2O_7$. All other reflections can be indexed on a smaller hexagonal subcell with $a = 5.268$ Å, $c = 13.076$ Å, $Z = 2$.

O atoms, all located on 4*a* sites of the $Pna2_1$ space group. A similar borate oxide model was also initially assumed and eventually confirmed for $SrBi_2B_2O_7$. In this case, however, several primitive hexagonal space groups had to be tested during the structure determination process. Similar global optimization results were obtained with several non-centrosymmetric space groups including *P*-6, *P*-62*m*, $P6_3$ and $P6_322$ which were used initially to solve the structure corresponding to the smaller hexagonal subcell identified in the powder X-ray pattern (Table 1). The final choice of the $P6_3$ space group for the description of the larger $a\sqrt{3}$ superstructure was based on the full refinement of the structure model.

The structure models for $CaBi_2B_2O_7$ and $SrBi_2B_2O_7$ were refined by the Rietveld method with the program FULL-PROF [18] using the neutron powder data. The refinement results are summarized in Table 2 and the final Rietveld profiles are shown in Fig. 1. The atomic coordinates and selected bond distances are listed in Tables 3 and 4, respectively. Soft distance constraints were applied to the B–O bonds in both structures (B–O = 1.37(1) Å). The refinement of the $CaBi_2B_2O_7$ structure proceeded smoothly and yielded adequate bonding environments for all atoms. The case of the $SrBi_2B_2O_7$ structure was more problematic as similar refinement statistics were obtained for the various hexagonal space groups mentioned earlier, in particular for *P*-6 and $P6_3$. The choice of the latter was eventually based on crystal chemical grounds whereby the $P6_3$ symmetry provides a simpler description of the $SrBi_2B_2O_7$ structure while maintaining a close analogy to that of $CaBi_2B_2O_7$. In both structures, the 6_3 or 2_1 screw axes make adjacent (001) layers crystallographically equivalent.

As revealed by the rather large B_{iso} parameters refined for all the atoms in the $SrBi_2B_2O_7$ structure, significant positional disorder is present in the $P6_3$ model which must be regarded as an average structure model only. In particular, the disorder is associated with the Bi atoms

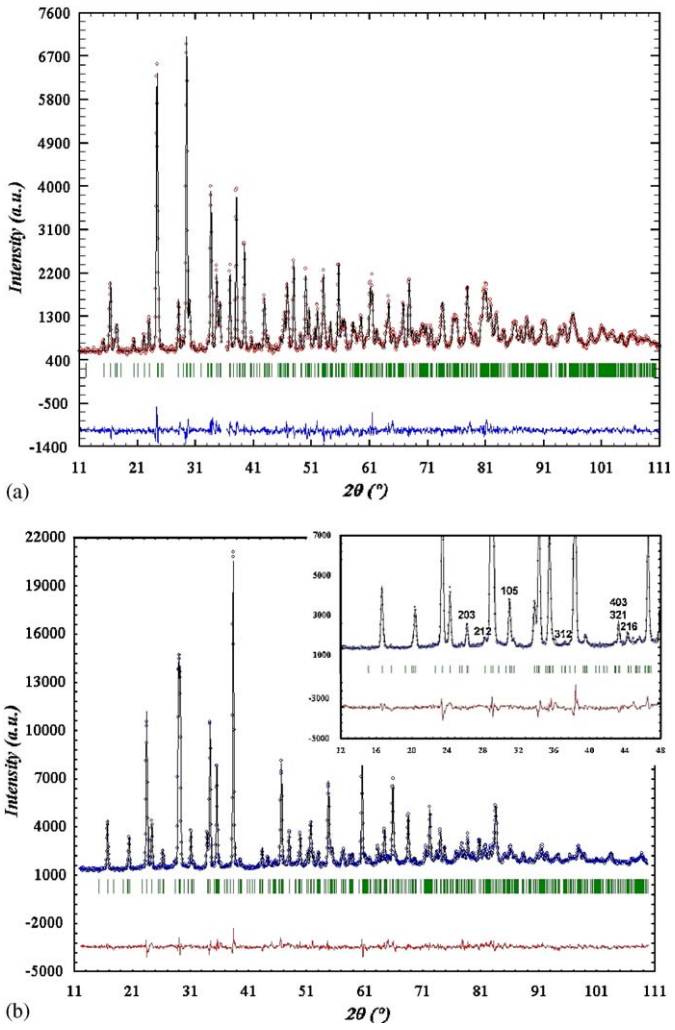

Fig. 1. Final profiles for the Rietveld refinements of $CaBi_2B_2O_7$ (a) and $SrBi_2B_2O_7$ (b). A minor impurity peak (800 counts at $2\theta = 36°$) has been excluded in (a). Some of the superstructure reflections are indexed in the inset in (b).

Table 2
Neutron Rietveld refinement results for $CaBi_2B_2O_7$ and $SrBi_2B_2O_7$

	$CaBi_2B_2O_7$	$SrBi_2B_2O_7$
Space group	$Pna2_1$	$P6_3$
Unit-cell	$a = 8.9371(5)$ Å	$a = 9.1404(4)$ Å
	$b = 5.4771(3)$ Å	—
	$c = 12.5912(7)$ Å	$c = 13.0808(6)$ Å
	$V = 616.33(6)$ Å^3	$V = 946.44(7)$ Å^3
Z	4	6
Neutron wavelength (Å)	1.33020	1.33025
Step size (deg)	0.05	0.05
2θ range (deg)	11.0–114.0	11.0–111.0
Excluded 2θ region (deg)	35.6–36.5	
No. of parameters	51	52
No. of unique reflections	674	651
R_{wp}	0.118	0.115
R_{exp}	0.078	0.057
χ^2	2.30	4.15
R_{Bragg}	0.047	0.063

which have unusually large B_{iso} parameters (3.5 Å^2) and inadequate coordination environments with long Bi–O bonds and low bond-valence sums (Table 4). Attempts to refine the structure in a lower symmetry space group, such as *P*3, did not yield any significant improvement. The tentative refinement of anisotropic displacement parameters for the Bi atoms gave a clear indication of a strong anisotropy with large displacement amplitudes perpendicular to the *c*-axis. Although it led to slightly better R indices, a non-positive definite parameter was obtained for one of the Bi atoms, possibly due to strong correlations during the refinement. Subsequently, several electron diffraction patterns recorded on microscopic crystals of $SrBi_2B_2O_7$ revealed the presence of additional very weak and diffuse reflections corresponding to a larger $2 \times a\sqrt{3}$ hexagonal superstructure (Fig. 2). Therefore, the large displacement parameters refined for the $SrBi_2B_2O_7$ model based on the smaller $a\sqrt{3}$ unit-cell can be explained by the averaging of atomic positions over sub-microscopic

Table 3
Atomic coordinates and isotropic displacement parameters for $CaBi_2B_2O_7$ ($Pna2_1$) and $SrBi_2B_2O_7$ ($P6_3$)

	x	y	z	B_{iso} (Å^2)[a]
Ca	−0.1743(8)	0.5508(15)	0.500[b]	1.14(15)
Bi1	0.1656(17)	0.431(2)	0.338(2)	0.87(6)
Bi2	0.1694(15)	0.444(2)	0.656(2)	0.87(6)
B1	0.4752(7)	0.4923(12)	0.6339(19)	0.74(6)
B2	0.4760(7)	0.4819(12)	0.3734(18)	0.74(6)
O1	−0.102(2)	0.796(2)	0.641(3)	0.94(4)
O2	0.1261(9)	0.038(4)	0.631(2)	0.94(4)
O3	0.392(2)	0.280(2)	0.635(2)	0.94(4)
O4	−0.095(2)	0.797(3)	0.361(2)	0.94(4)
O5	0.1283(9)	0.043(4)	0.377(2)	0.94(4)
O6	0.390(2)	0.274(3)	0.375(2)	0.94(4)
O7	0.1333(6)	0.5306(11)	0.500[b]	0.94(4)
Sr	0.9642(8)	0.3161(15)	0.000[b]	1.94(12)
Bi1	0.322(3)	0.339(3)	0.8402(15)	3.5(3)
Bi2	0.336(3)	0.344(3)	0.1650(16)	3.6(3)
B1	0.00000	0.00000	0.127(2)	1.25(6)
B2	0.33333	0.66667	0.1172(18)	1.25(6)
B3	0.66667	0.33333	0.1637(16)	1.25(6)
B4	0.00000	0.00000	0.361(2)	1.25(6)
B5	0.33333	0.66667	0.3509(16)	1.25(6)
B6	0.66667	0.33333	0.3677(19)	1.25(6)
O1	0.134(2)	−0.138(2)	0.134(2)	2.19(5)
O2	0.329(3)	0.8132(18)	0.1274(19)	2.19(5)
O3	0.816(2)	0.334(4)	0.150(2)	2.19(5)
O4	−0.1429(19)	0.013(3)	0.359(3)	2.19(5)
O5	0.327(4)	0.514(2)	0.343(2)	2.19(5)
O6	0.5259(16)	0.349(3)	0.3743(19)	2.19(5)
O7	0.3698(13)	0.330(2)	0.000[b]	2.19(5)

[a] B parameters constrained for atoms of a given type.
[b] The z(Ca) and z(Sr) coordinates were used to fix the origin in the z direction. The $z(O_7)$ coordinates did not deviate significantly from the ideal values of 0.50 (Ca) and 0.00 (Sr).

Table 4
Selected bond lengths (l, Å) and bond valences (s)[a] in $CaBi_2B_2O_7$ and $SrBi_2B_2O_7$

	l	s
$CaBi_2B_2O_7$		
Ca–O1	2.32(3)	0.385
Ca–O4	2.32(2)	0.385
Ca–O2	2.47(2)	0.257
Ca–O5	2.40(2)	0.310
Ca–O3	2.56(2)	0.201
Ca–O6	2.45(2)	0.271
Ca–O7	2.751(9)	0.120
Ca–O7	2.865(10)	0.088
Σs		2.02
Bi1–O1	2.83(4)	0.136
Bi1–O4	3.09(2)	0.066
Bi1–O4	2.63(3)	0.249
Bi1–O5	2.21(3)	0.736
Bi1–O6	2.23(2)	0.693
Bi1–O6	2.75(2)	0.171
Bi1–O7	2.14(5)	0.905
Σs		2.96
Bi2–O1	3.11(2)	0.068
Bi2–O1	2.50(2)	0.324
Bi2–O4	2.97(3)	0.092
Bi2–O2	2.28(2)	0.604
Bi2–O3	2.20(2)	0.751
Bi2–O3	2.78(2)	0.157
Bi2–O7	2.05(3)	1.141
Σs		3.14
B1–O1	1.355(15)	1.044
B1–O2	1.359(10)	1.033
B1–O3	1.379(15)	0.979
Σs		3.06
B2–O4	1.375(18)	0.989
B2–O5	1.368(11)	1.008
B2–O6	1.373(17)	0.995
Σs		2.99
Bi1–O7–Bi2	147.0(23)	
SrBi2B2O7		
Sr–O1	2.48(2)	0.376
Sr–O2	2.56(2)	0.306
Sr–O3	2.44(3)	0.424
Sr–O4	2.53(3)	0.329
Sr–O5	2.50(3)	0.351
Sr–O6	2.54(2)	0.323
Sr–O7	2.61(2)	0.264
Sr–O7	2.89(2)	0.124
Σs		2.50
Bi1–O1	3.18(3)	0.053
Bi1–O3	2.95((3)	0.099
Bi1–O4	2.80(3)	0.148
Bi1–O4	2.47(3)	0.362
Bi1–O5	2.79(3)	0.152
Bi1—O5	2.73(3)	0.179
Bi1–O6	2.67(3)	0.211
Bi1–O6	2.51(3)	0.325
Bi1–O7	2.15(2)	0.860
Σs		2.39
Bi2–O1	2.92(3)	0.107
Bi2–O1	2.53(3)	0.302
Bi2–O2	2.59(4)	0.262
Bi2–O2	2.64(3)	0.230
Bi2–O3	2.64(4)	0.234
Bi2–O3	2.71(4)	0.186
Bi2–O4	3.08(4)	0.070
Bi2–O5	2.83(3)	0.139
Bi2–O7	2.19(2)	0.765
Σs		2.29
B1–O1	1.370(15) × 3	
B2–O2	1.367(20) × 3	
B3–O3	1.373(26) × 3	
B4–O4	1.370(19) × 3	
B5–O5	1.373(18) × 3	
B6–O6	1.365(18) × 3	
Bi1–O7–Bi2	156.8(17)	

[a] Bond valence parameters from Ref. [20].

domains corresponding to the double superstructure with different orientations. The diffuse reflections associated with this short-range superstructure remain unobservable in either the X-ray or neutron powder diffraction patterns. Even after annealing a powder sample at 500 °C for 1 week, no evidence of the larger superstructure could be detected by powder X-ray diffraction.

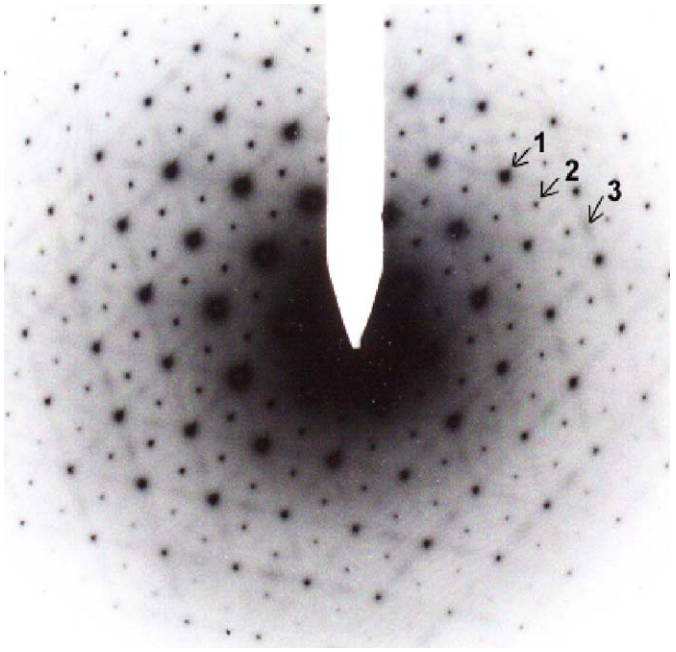

Fig. 2. Electron diffraction pattern of $SrBi_2B_2O_7$ recorded along the [001] zone axis. Note the strong hexagonal sub-cell (type 1 reflections), the weak and sharp $a\sqrt{3}$ superstructure (type 2) and the very weak and diffuse $2a\sqrt{3}$ superstructure (type 3).

3. Description of the $CaBi_2B_2O_7$ and $SrBi_2B_2O_7$ structures

Both compounds belong to the same novel borate oxide structure type, $MBi_2O(BO_3)_2$, corresponding to a stacking of stoichiometric layers built of corner-sharing BO_3 triangles and MO_6 trigonal prisms with Bi_2O groups accommodated within six-membered rings (Fig. 3a). The layers are stacked along the c direction in a staggered configuration so that the Bi atoms in one layer are weakly bonded to the O atoms of a MO_6 trigonal prism in the adjacent layer (Fig. 3b). The layer nature of the structures and the weak bonding interactions between the neutral layers account for the fragility and easy cleavage observed in single crystals.

The alternating BO_3 triangles and MO_6 trigonal prisms forming the six-membered rings within individual (001) layers yield a noncentrosymmetric arrangement. In both structures, adjacent layers are symmetrically equivalent and related to each other via the 2_1 (Ca) and 6_3 (Sr) screw axes parallel to the c direction, so that the overall structures are also noncentrosymmetric. The bent geometries of the $Bi–O_7–Bi_2$ groups (Table 4) also contribute to the noncentrosymmetric character of each structure. It is noteworthy that the larger $Bi–O_7–Bi_2$ angle in $SrBi_2B_2O_7$ correlates with the larger volume of the SrO_6 trigonal prisms and the associated expansion of the unit-cell along the c-axis (Table 2).

The main differences between the $CaBi_2B_2O_7$ and $SrBi_2B_2O_7$ structures arise from the orthorhombic and hexagonal symmetry, respectively, of their $MBi_2B_2O_7$ layers. In $CaBi_2B_2O_7$ (Fig. 4a), the orthorhombic lattice

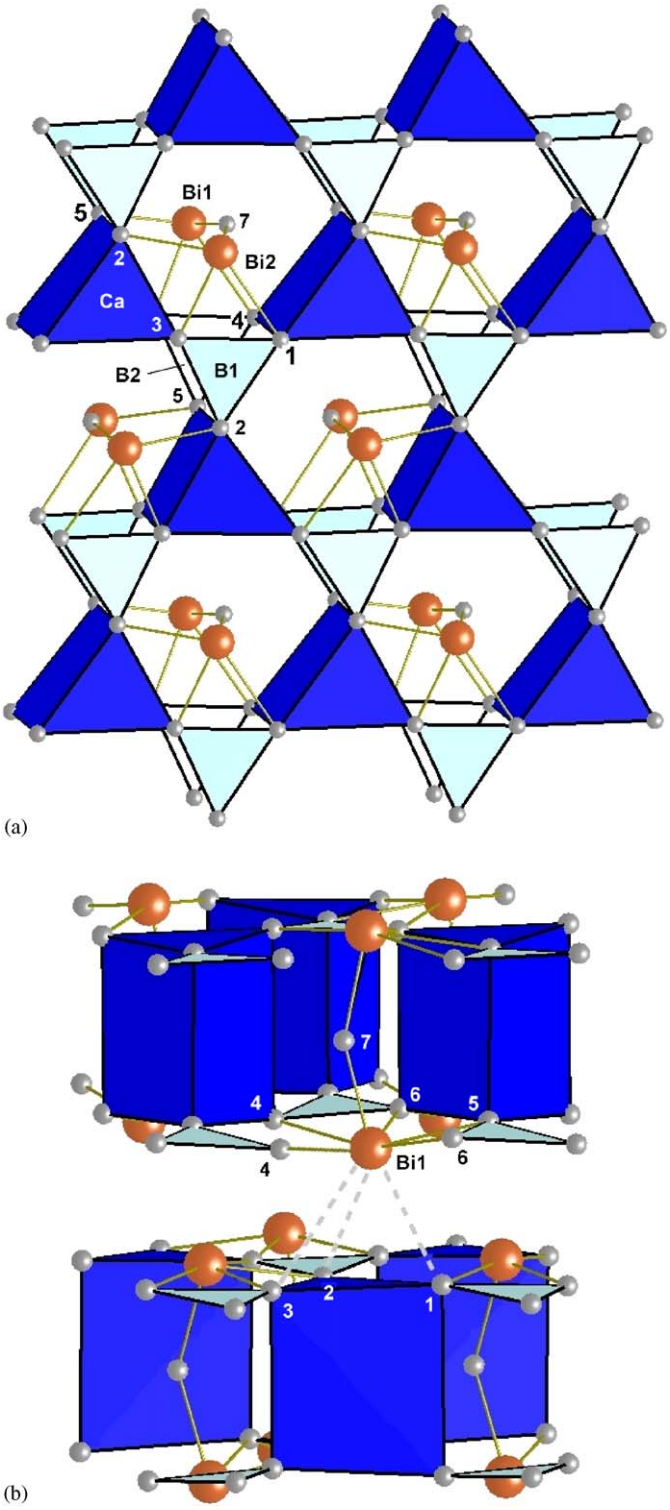

Fig. 3. (a) A single layer in the $CaBi_2B_2O_7$ structure viewed approximately along the c-axis. (b) Two adjacent layers in the $CaBi_2B_2O_7$ structure viewed approximately perpendicular to the c-axis. Dashed lines represent long and weak inter-layer Bi–O bonds (2.82–3.25 Å). Numbers correspond to the O atoms. The $SrBi_2B_2O_7$ structure is based on a similar layer stacking.

distortion occurs in the (001) plane as shown by the a/b-axis ratio (1.632) which is significantly smaller than the ideal value of $\sqrt{3}$. This distortion is primarily achieved via

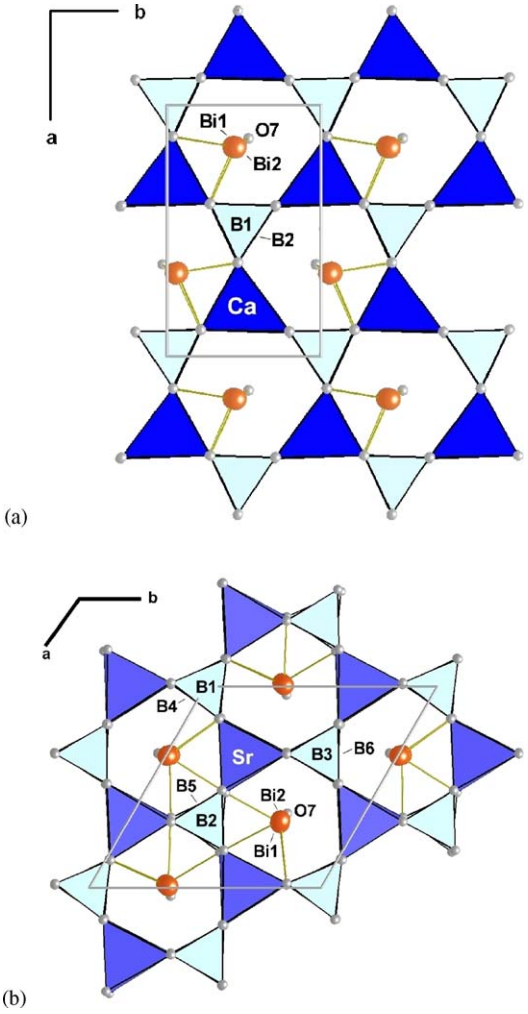

Fig. 4. The (001) projections of a single layer in the $CaBi_2B_2O_7$ (a) and $SrBi_2B_2O_7$ (b) structures. The thin lines represent the intra-layer Bi–O bonds shorter than 2.3 Å (Ca) and 2.6 Å (Sr).

the loss of trigonal symmetry in the CaO_6 prisms and the off-center shifts of the Bi atoms within the six-membered rings. These shifts result in strongly asymmetric coordination environments for Bi1 and Bi2, with three short Bi–O bonds in each case that yield proper bond valence sums (Table 4). In $SrBi_2B_2O_7$ (Fig. 4b), the hexagonal lattice symmetry is retained but a minor ditrigonal distortion of the six-membered rings leads to the formation of the $a\sqrt{3}$ superstructure. The Bi atoms remain located near the center of the rings with a more symmetrical coordination environment containing one short Bi–O_7 bond and eight much longer Bi–O bonds (Table 4). As a result, the bond valence sums for Bi1 (2.39) and Bi2 (2.29) are much lower than expected and indicate a significant underbonding for these atoms. Simultaneously, the bond valence sum for Sr (2.50) indicates overbonding. These strong deviations in the bond valence sums suggest that the refined model for $SrBi_2B_2O_7$ is only an approximation of the true structure, as was also indicated by the large B_{iso} parameters (Table 3) and the observation of a larger $2 \times a\sqrt{3}$ superstructure in electron diffraction patterns (Fig. 2). This superstructure can arise through concerted rotations of the BO_3 groups within the basal plane of the structure, as well as through concerted shifts of the Bi atoms within the rings (Fig. 4b). The associated atom displacements could readily lead to shortening and lengthening of some Bi–O and Sr–O bonds, respectively, thereby yielding more adequate coordination environments and bond valence sums for the Bi and Sr atoms.

In spite of the average nature of the structure model refined for $SrBi_2B_2O_7$ in the present study, it is clear from the Rietveld refinement results that the model is essentially correct and that both $SrBi_2B_2O_7$ and $CaBi_2B_2O_7$ crystallize with the same layer structure-type. The larger size of the Sr^{2+} cation may correspond to an upper limit for the stability field of this structure-type as suggested by the absence of an analogous compound in the $BaO–Bi_2O_3–B_2O_3$ system [15].

4. Second harmonic generation (SHG) properties

On the basis of their non-centrosymmetric crystal structures, both $CaBi_2B_2O_7$ and $SrBi_2B_2O_7$ are expected to possess NLO properties. This was confirmed in the case of $CaBi_2B_2O_7$ by measuring its efficiency for SHG (d_{eff}). A powder sample with a grain size in the 50–75 μm range was used in a Kurtz–Perry-type instrument which has been described elsewhere [19]. The measurement of the SHG efficiency relative to a KH_2PO_4 (KDP) standard with the same grain size gave a value of d_{eff} ($CaBi_2B_2O_7$) = 2.00d_{eff} (KDP).

The moderate SHG efficiency measured for $CaBi_2B_2O_7$ is in agreement with the details of its crystal structure. The nearly coplanar array of BO_3 triangles within each layer of the structure would favour a large d_{eff} value but their alignment perpendicular to the polar c-axis and their different orientations in adjacent layers (Fig. 3b) can be expected to reduce their overall contribution to the NLO properties [21]. Similarly, the geometry of the $O_nBi–O_7–Bi_2O_n$ groups can be expected to yield only a small dipole moment for each bismuthate dimer and their opposite orientations in adjacent layers decreases their net contribution further. For similar reasons, the $SrBi_2B_2O_7$ structure is expected to also display only a moderate SHG efficiency.

5. Conclusion

The two compounds, $MBi_2B_2O_7$ or $MBi_2O(BO_3)_2$ (M = Ca, Sr), represent a novel non-centrosymmetric structure-type for borate oxides consisting of a stacking of identical neutral layers bridged by weak Bi–O bonds. The orientations of the BO_3 and Bi_2O_n groups within each crystal structure result in moderate second harmonic generation (SHG) properties. Future work will investigate the extension of the new structure-type through substitution by other M^{2+} ions and formation of solid solutions. As well, the possibility to replace the Bi_2O^{4+} groups within the rings with other cationic species will be explored.

Acknowledgments

The Canadian Neutron Beam Centre in Chalk River, Ontario, is gratefully acknowledged for time granted on the C2 high-resolution powder neutron diffractometer. P. Elder in Prof. Vargas-Baca's research group at McMaster University is also acknowledged for carrying out the measurement of the SHG efficiency of $CaBi_2B_2O_7$.

Finally, the authors are grateful for useful comments by anonymous referees.

References

[1] H. Hellwig, J. Liebertz, L. Bohaty, Solid State Commun. 109 (1998) 249–251.
[2] Z. Lin, Z. Wang, C. Chen, M.-H. Lee, J. Appl. Phys. 90 (2001) 5585–5590.
[3] B. Teng, J. Wang, Z. Wang, X. Hu, H. Jiang, H. Liu, X. Cheng, S. Dong, Y. Liu, J. Shao, J. Cryst. Growth 233 (2001) 282–286.
[4] R. Frohlich, L. Bohaty, J. Liebertz, Acta Crystallogr. C 40 (1984) 343.
[5] P. Becker, R. Froehlich, Z. Naturforsch. B 59 (2004) 256–258.
[6] A. Hyman, A. Perloff, Acta Crystallogr. B 28 (1972) 2007.
[7] M. Muehlberg, M. Burianek, H. Edongue, Ch. Poetsch, J. Cryst. Growth 237–239 (2002) 740–744.
[8] B. Teng, W.T. Yu, J.Y. Wang, X.F. Cheng, S.M. Dong, Y.G. Liu, Acta Crystallogr. C 58 (2002) i25.
[9] S. Filatov, Y. Shepelev, R. Bubnova, N. Sennova, A.V. Egorysheva, Y.F. Kargin, J. Solid State Chem. 177 (2004) 515–522.
[10] L. Li, G. Li, Y. Wang, F. Liao, J. Lin, Inorg. Chem. 44 (2005) 8243–8248.
[11] L. Li, G. Li, Y. Wang, F. Liao, J. Lin, Chem. Mater. 17 (2005) 4174–4180.
[12] G.A. Petrakovskii, A.M. Vorotynov, K.A. Sablina, L.V. Udod, A.I. Pankrats, C.J. Ritter, J. Magn. Magn. Mater. 263 (2003) 245–248.
[13] M.I. Zargarova, M.F. Kasumova, G.K. Abdullaev, Russ. J. Inorg. Chem. 32 (1987) 737.
[14] X. Chen, J. Zuo, X. Chang, Y. Zhao, H. Zang, W. Xiao, J. Solid Sate Chem. 179 (2006) 3191–3195.
[15] J. Barbier, N. Penin, A. Denoyer, L.M.D. Cranswick, Solid State Sci. 7 (2005) 1055–1061.
[16] J. Barbier, N. Penin, L.M.D. Cranswick, Chem. Mater. 17 (2005) 3130–3136.
[17] R. Cerny, V. Favre-Nicolin, Powder Diffr. 20 (2005) 359–365.
[18] J. Rodriguez-Carvajal, FULLPROF version 2.55 (2004), Institut Laue-Langevin, Grenoble, France.
[19] H. Park, A. Bakhtiiarov, W. Zhang, I. Vargas-Baca, J. Barbier, J. Solid State Chem. 177 (2004) 159–164.
[20] N.E. Brese, M. O'Keeffe, Acta Crystallogr. B 47 (1991) 192–197.
[21] P. Becker, Adv. Mater. 10 (1998) 979–992.